JOURNAL OF APPLIED CRYSTALLOGRAPHY

Volume 50 (2017)

Supporting information for article:

Determination of active layer morphology in all-polymer photovoltaic cells

Andrew J. Mulderig, Yan Jin, Fei Yu, Jong Keum, Kunlun Hong, James F. Browning, Gregory Beaucage, Gregory S. Smith and Vikram K. Kuppa

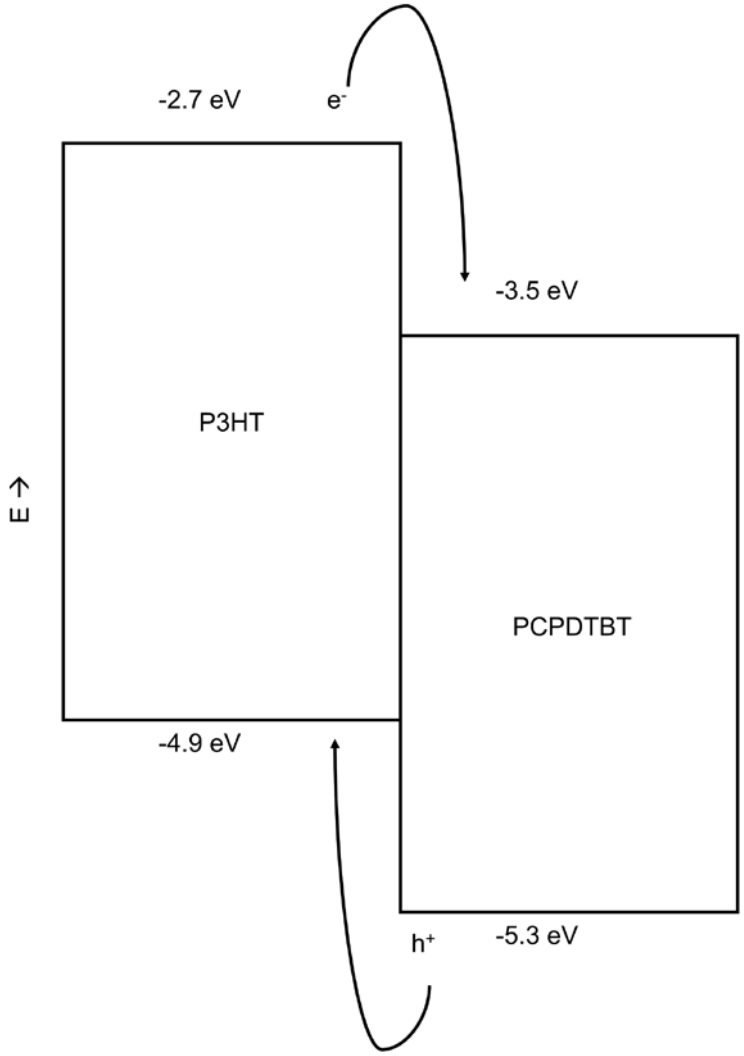

Figure S1 Energy level diagram for P3HT/PCPDTBT blends (Shao et al., 2014; Soci et al., 2007).

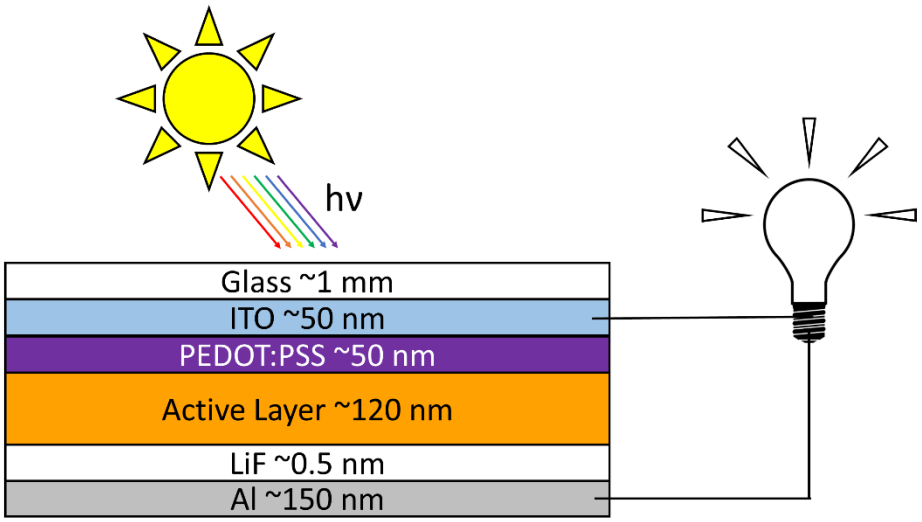

Figure S2 Layer stack of P3HT/PCPDTBT OPV devices. Poly(2,3-dihydrothieno-1,4-dioxin)-poly(styrenesulfonate), PEDOT:PSS, was spin-coated onto glass slides patterned with indium tin oxide, ITO. The P3HT/PCPDTBT active layer solution was then spin-coated on top of the PEDOT:PSS layer. Finally, a thin layer of lithium fluoride and the aluminium back electrode were sputtered onto the active layer film.

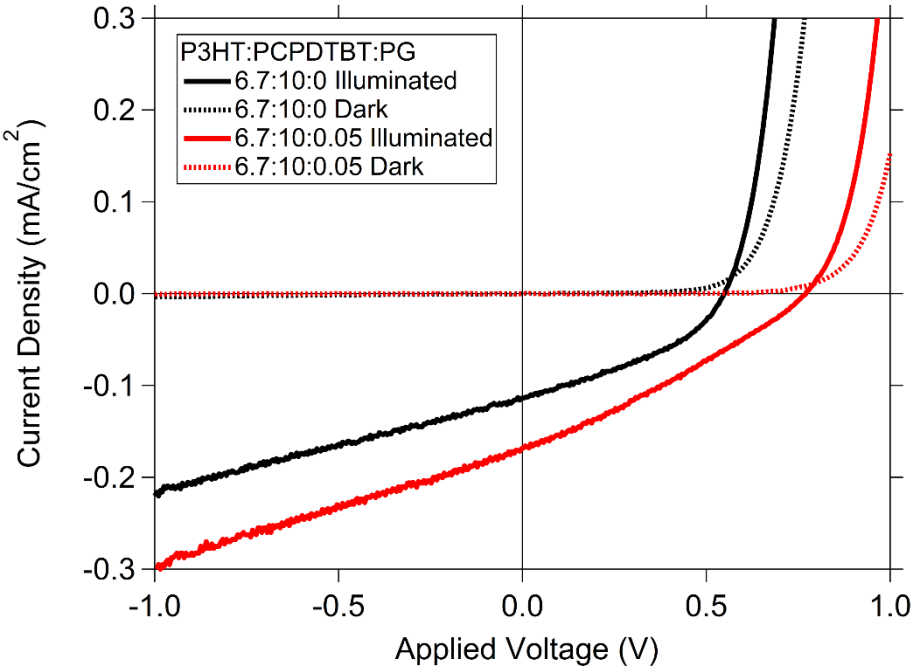

Figure S3 Example J-V curves from OPV devices consisting of 40:60 P3HT/PCPDTBT blends without (black curves) and with (red curves) the PG additive. Photovoltaic devices were tested under 100 mW/cm^2 illumination using an AM1.5G filter to match the solar emission spectrum and intensity. The same solar cells were tested in dark conditions (dotted lines) to establish baseline diode behaviour. The addition of 0.3 wt% PG results in increased V_{oc}, J_{sc}, FF and η for the 40:60 P3HT/PCPDTBT solar cells.

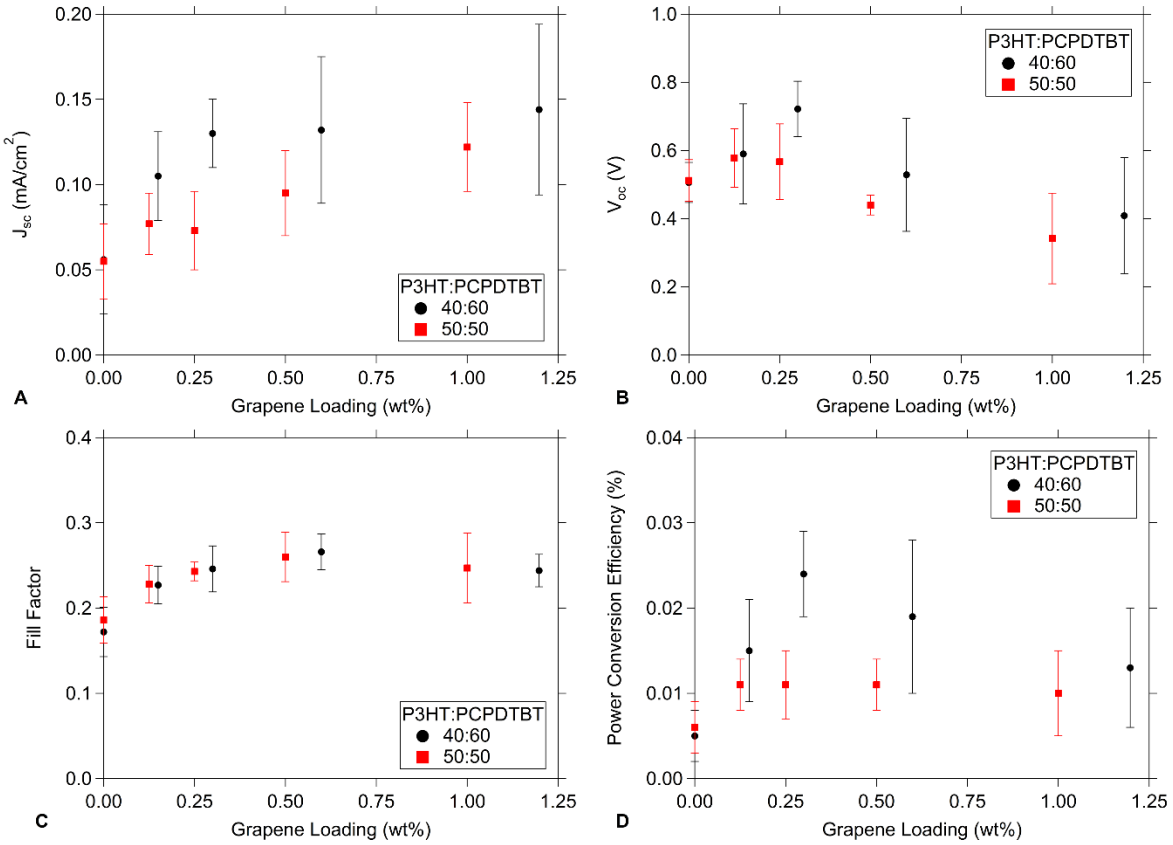

Figure S4 J_{sc} (A), V_{oc} (B), FF (C) & η (D) for 40:60 (circles) and 50:50 (squares) P3HT/PCPDTBT OPV devices with various PG loading. Each data point represents the average of at least six OPV devices and the error bars show the standard deviation of the performance metric for the data set.

Figure S4 shows short-circuit current density (A), open circuit voltage (B), fill factor (C) and power conversation efficiency (D) of 40:60 and 50:50 P3HT/PCPDTBT all-polymer solar cells with various PG loadings. For both polymer ratios tested, V_{oc} increases to a maximum at low PG loading (0.125% for 50:50 and 0.3% for 40:60 samples) then decreases for samples of higher PG weight fraction. However, the large standard deviation error bars suggest that these results are statistically similar. J_{sc} seems to generally increase with increasing PG loading; this is the expected trend due to the high ambipolar charge carrier mobility of the graphene sheets assisting charge transport in the composite active layer. On average, FF increased from the values obtained for neat samples (without PG additive) for both 40:60 and 50:50 samples, indicative of improved charge transport (Facchetti, 2013). Power conversion efficiency seemed to increase to a maximum at low graphene loading then decrease for samples of higher PG weight fraction, following the trend in J_{sc}. Although the power conversion efficiency of the 50:50 P3HT/PCPDTBT OPV devices with PG is not significantly different from the neat cells, the 40:60 samples with 0.3% PG showed significantly higher performance (greater than one standard deviation) compared to the neat cells. This relative performance increase is on par with that seen by Fei Yu in P3HT/PCBM devices (Yu & Kuppa, 2013) with graphene and Yan Jin in P3HT/F8BT devices (Jin, Yu & Kuppa, 2015).

Table S1 Mean and standard deviation values for J_{sc}, V_{oc}, FF & η for 40:60 and 50:50 P3HT/PCPDTBT OPV devices with various PG loading.

	PG Loading	**J_{sc} (mA/cm^2)**	**V_{oc} (V)**	**FF**	**η**
40:60	0.00 wt%	0.06 ± 0.03	0.51 ± 0.06	0.17 ± 0.03	0.005% ± 0.003%
	0.15 wt%	0.11 ± 0.03	0.59 ± 0.15	0.23 ± 0.02	0.015% ± 0.006%
	0.30 wt%	0.13 ± 0.02	0.72 ± 0.08	0.25 ± 0.03	0.024% ± 0.005%
	0.60 wt%	0.13 ± 0.04	0.53 ± 0.17	0.27 ± 0.02	0.019% ± 0.009%
	1.20 wt%	0.14 ± 0.05	0.41 ± 0.17	0.24 ± 0.02	0.013% ± 0.007%
50:50	0.00 wt%	0.06 ± 0.02	0.51 ± 0.06	0.19 ± 0.03	0.006% ± 0.003%
	0.13 wt%	0.08 ± 0.02	0.58 ± 0.09	0.23 ± 0.02	0.011% ± 0.003%
	0.25 wt%	0.07 ± 0.02	0.57 ± 0.11	0.24 ± 0.01	0.011% ± 0.004%
	0.50 wt%	0.10 ± 0.03	0.44 ± 0.03	0.26 ± 0.03	0.011% ± 0.003%
	1.00 wt%	0.12 ± 0.03	0.34 ± 0.13	0.25 ± 0.04	0.010% ± 0.005%

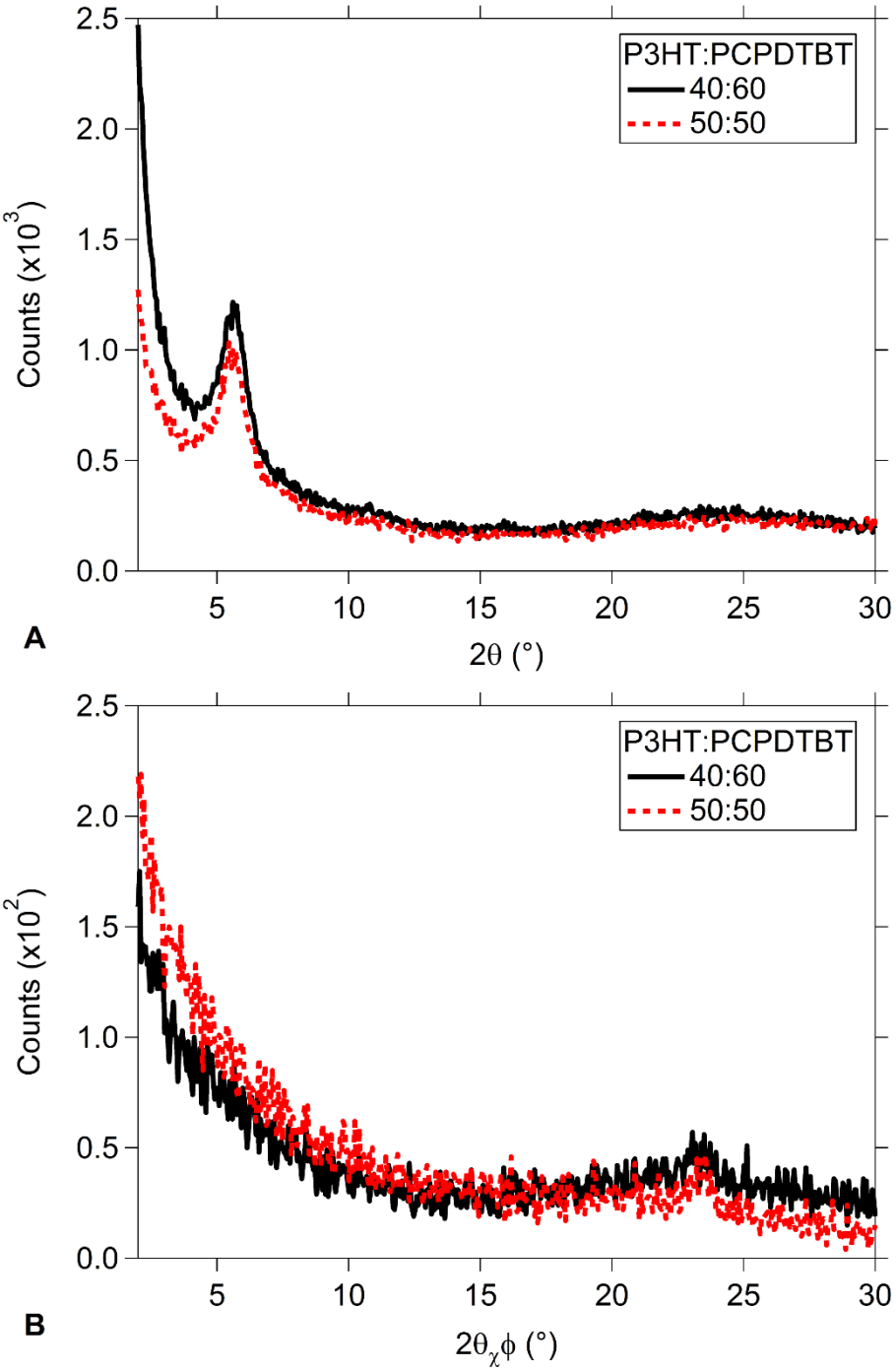

Figure S5 Out-of-plane (A) and in-plane (B) grazing incidence X-Ray diffraction data for 40:60 and 50:50 P3HT/PCPDTBT samples. The peak at about 2θ = 5.5° in the out-of-plane data matches results from literature for the (100) peak of P3HT (Chen *et al.*, 2013; Keum et al., 2013b; Kohn *et al.*, 2013). Although PCPDTBT crystallization has been reported in the literature (Agostinelli *et al.*, 2011; Gu, Wang & Russell, 2012) with a (100) peak at about 12°, no evidence of PCPDTBT crystallization is observed in our data. Despite the clear (100) reflection, similar (h00) reflections are not easily observed due to the suppressed crystallinity of the blend compared to pure P3HT. A similar phenomenon is observed from the in-plane GIXRD data in which a weak (020) peak at roughly 2θ =

23.2° is measured and compared with results from the literature (Chen *et al*., 2013; Keum *et al.*, 2013b; Kohn *et al*., 2013).

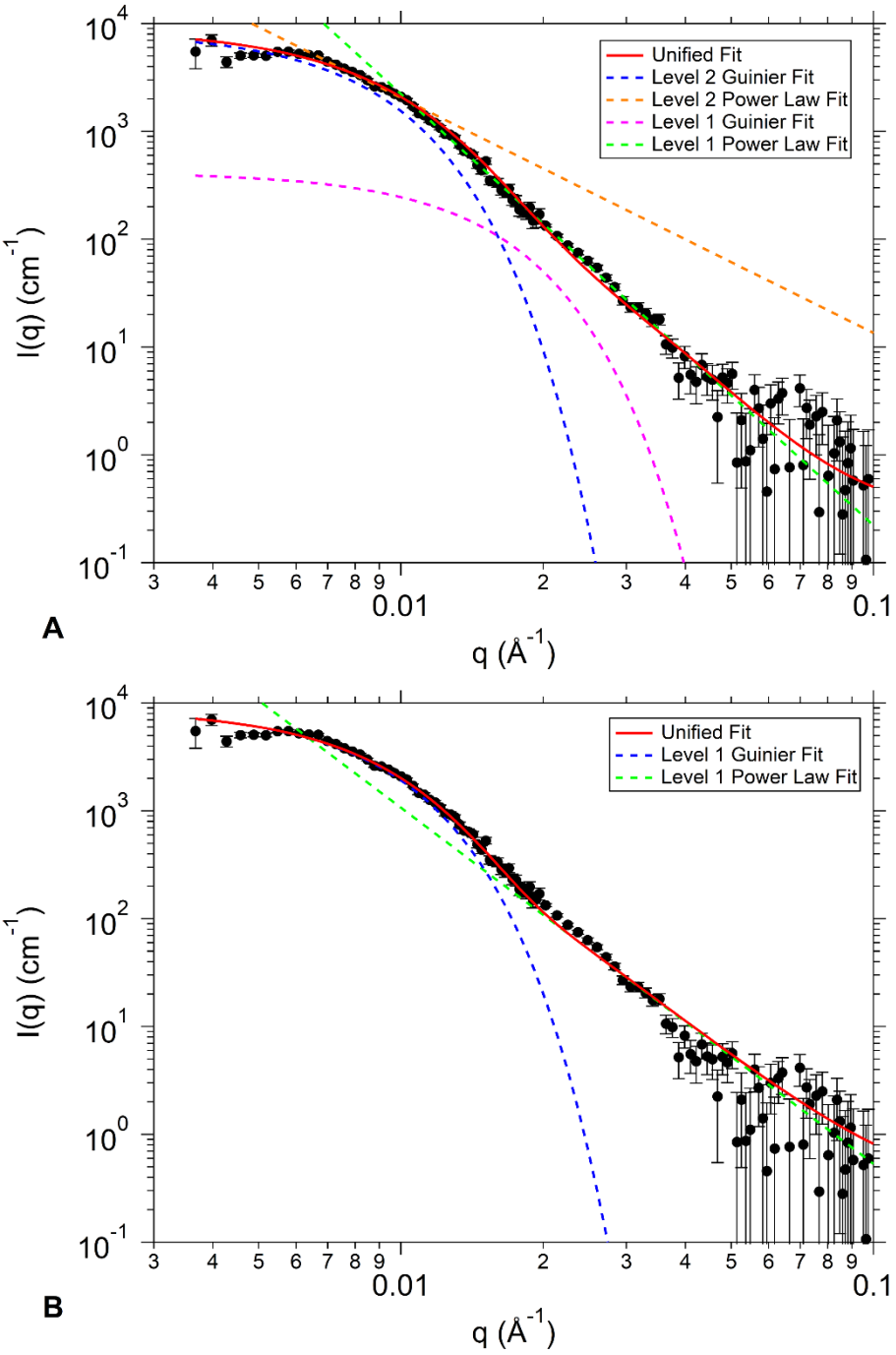

Figure S6 (A) Example fit of the unified scattering function (red curve) to the SANS data using two structural levels for the neat 50:50 sample (without PG). Dashed curves show the component Guinier and power law fits comprising the Unified fit. (B) A one-level Unified fit to the scattering data was attempted but the fit quality was poor in comparison to the two-level fit shown in Figure S6A.

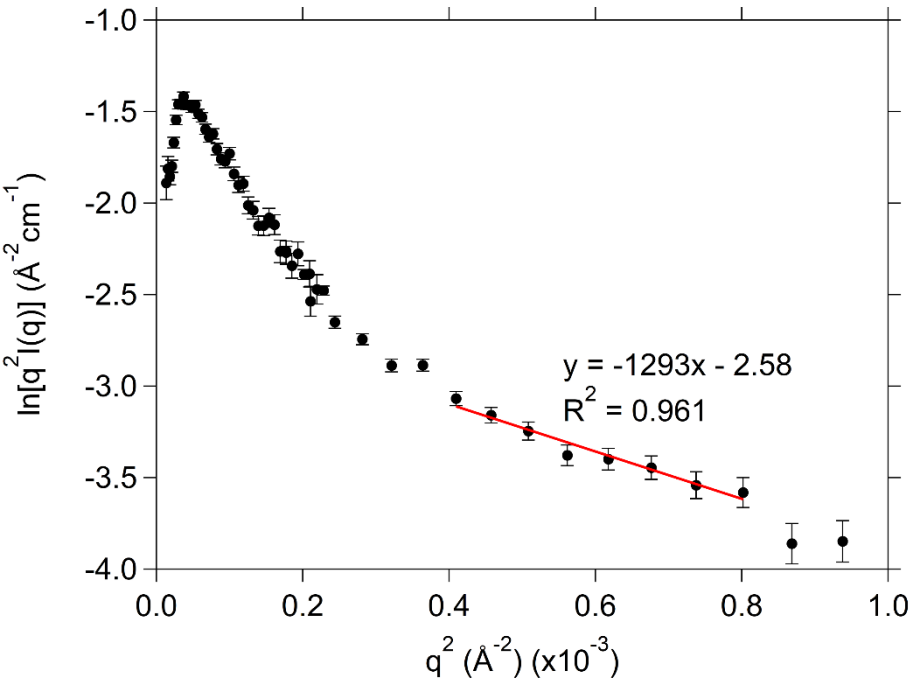

Figure S7 Example fit of the modified Guinier's law for flat objects in the medium-q regime for the neat 50:50 sample (without graphene). The limited range over which the fit is performed is required to satisfy the criterion $q \times R_g \leq 1$.

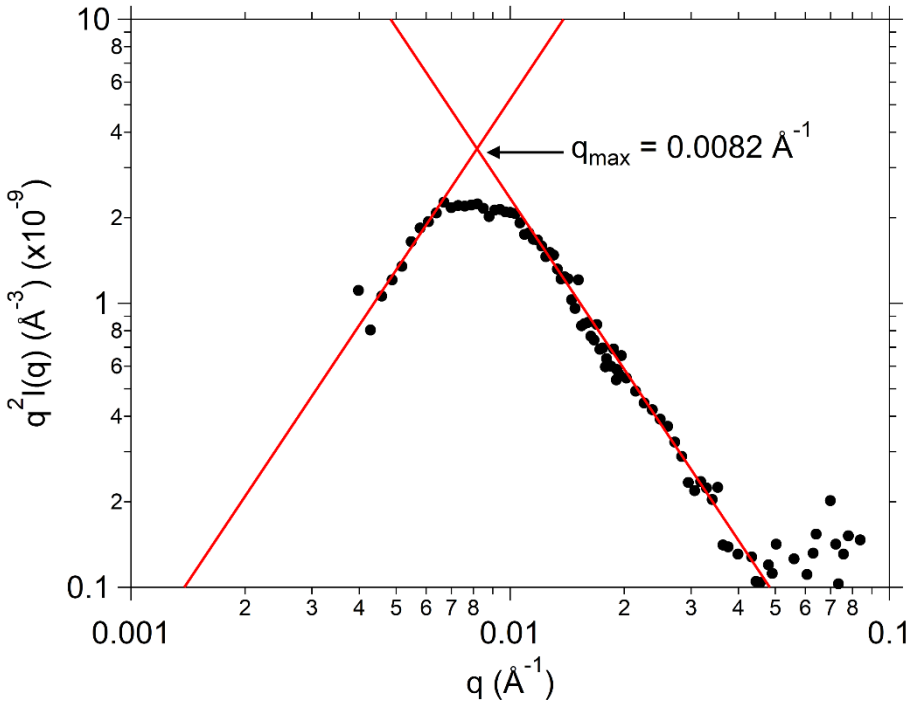

Figure S8 Example of power laws fit to both sides of the peak in the Kratky plot for the neat 40:60 sample. A power law 2 slope was fit on the left side of the peak and a power law -2 slope was fit to the right side of the peak. From the intersection of the two power laws, the position of the maximum, q_{max} = 0.0082 Å^{-1}, is obtained. This method was used since there is a power law slope of α = 0 in the low-q regime and a power law slope of α = -4 in the high-q regime of the scattering curves for all samples.

Table S2 Position of maximum in Kratky plots scattering pattern and calculated long period (L) for P3HT/PCPDTBT samples. Peak positions were determined by fitting a power law to the slopes on each side of the peak and recording the point of intersection.

	PG Loading	As-Cast		Annealed	
		q_{max} (Å^{-1})	L (nm)	q_{max} (Å^{-1})	L (nm)
40:60	0.00 wt%	0.0082 ± 0.0007	76.7 ± 5.8	0.0088 ± 0.0007	71.5 ± 5.4
	0.06 wt%	0.0082 ± 0.0006	76.7 ± 5.8	0.0076 ± 0.0006	82.9 ± 6.2
	0.15 wt%	0.0079 ± 0.0006	79.6 ± 6.0	0.0076 ± 0.0006	82.9 ± 6.2
	0.45 wt%	0.0082 ± 0.0006	76.7 ± 5.8	0.0079 ± 0.0006	79.8 ± 6.0
50:50	0.00 wt%	0.0076 ± 0.0005	82.8 ± 6.2	0.0073 ± 0.0006	86.2 ± 6.5
	0.05 wt%	0.0070 ± 0.0006	89.9 ± 6.8	0.0073 ± 0.0006	86.2 ± 6.5
	0.12 wt%	0.0070 ± 0.0005	89.9 ± 6.8	0.0070 ± 0.0005	89.9 ± 6.8
	0.37 wt%	0.0073 ± 0.0006	86.2 ± 6.5	0.0070 ± 0.0005	90.1 ± 6.8

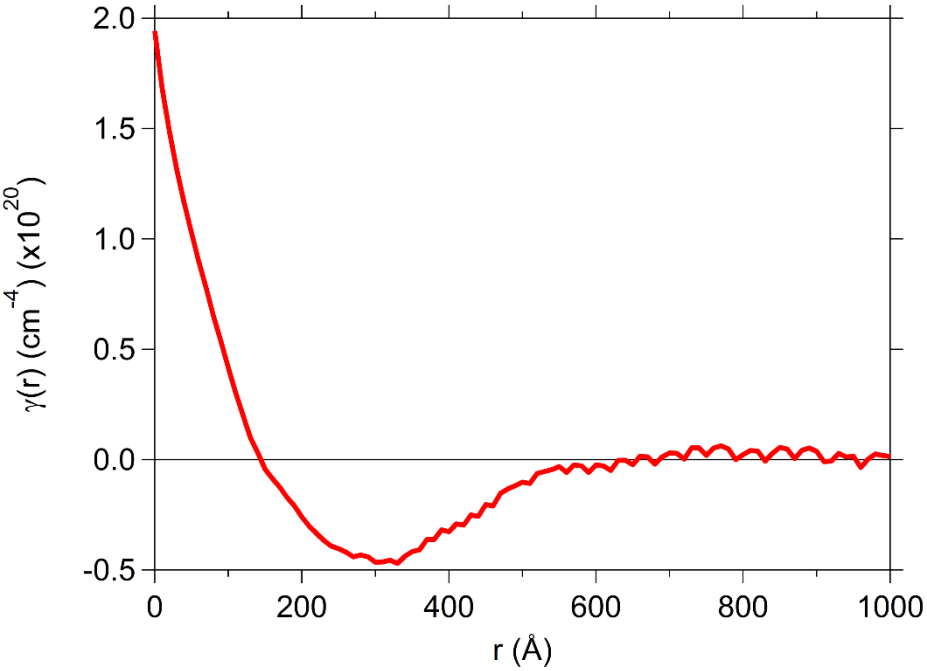

Figure S9 Example correlation function, γ(r), plotted with a step size of r = 10 Å for the neat 40:60 sample. Integration of Equation 8 was performed using trapezoids. Despite using Guinier's Law and Porod's Law to extrapolate to zero and infinity, respectively, integration errors appear at longer length scales.

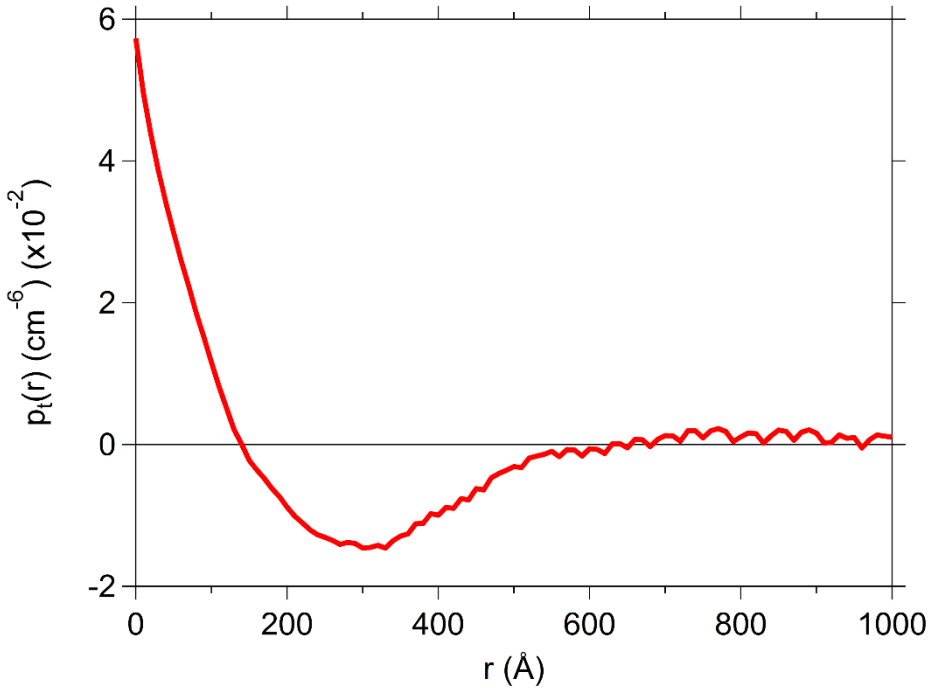

Figure S10 Example of a $p_t(r)$ plotted with a step size of r = 10 Å for the neat 40:60 sample. Integration of Equation S1 was performed using trapezoids. Despite using Guinier's Law and Porod's Law to extrapolate to zero and infinity, respectively, integration errors appear at longer length scales.

If the scattering particles are elongated in two dimensions, such as disks or lamellae, the thickness pair distance distribution function, $p_t(r)$, shown in Equation S1, can be used to obtain t from the scattered intensity of the cross section, $I_t(q)$ (Glatter, 1980; Glatter & Kratky, 1982).

$$p_t(r) = \frac{1}{\pi}\int_0^\infty I_t(q)\cos(qr)\,dq = \frac{1}{2\pi^3 R^2}\int_0^\infty q^2 I(q)\cos(qr)\,dq \qquad \text{(S1)}$$

If the basal plane of the scattering particle is flat, $p_t(r)$ should show a linear decrease with r. At a distance r = t, $p_t(r)$ decreases to zero because it is no longer possible for both volume elements to lie within the scattering particle. This data corroborates the two-dimensional nature of the P3HT crystallites in the P3HT/PCPDTBT films (Glatter & Kratky, 1982; Willerich & Gröhn, 2008).

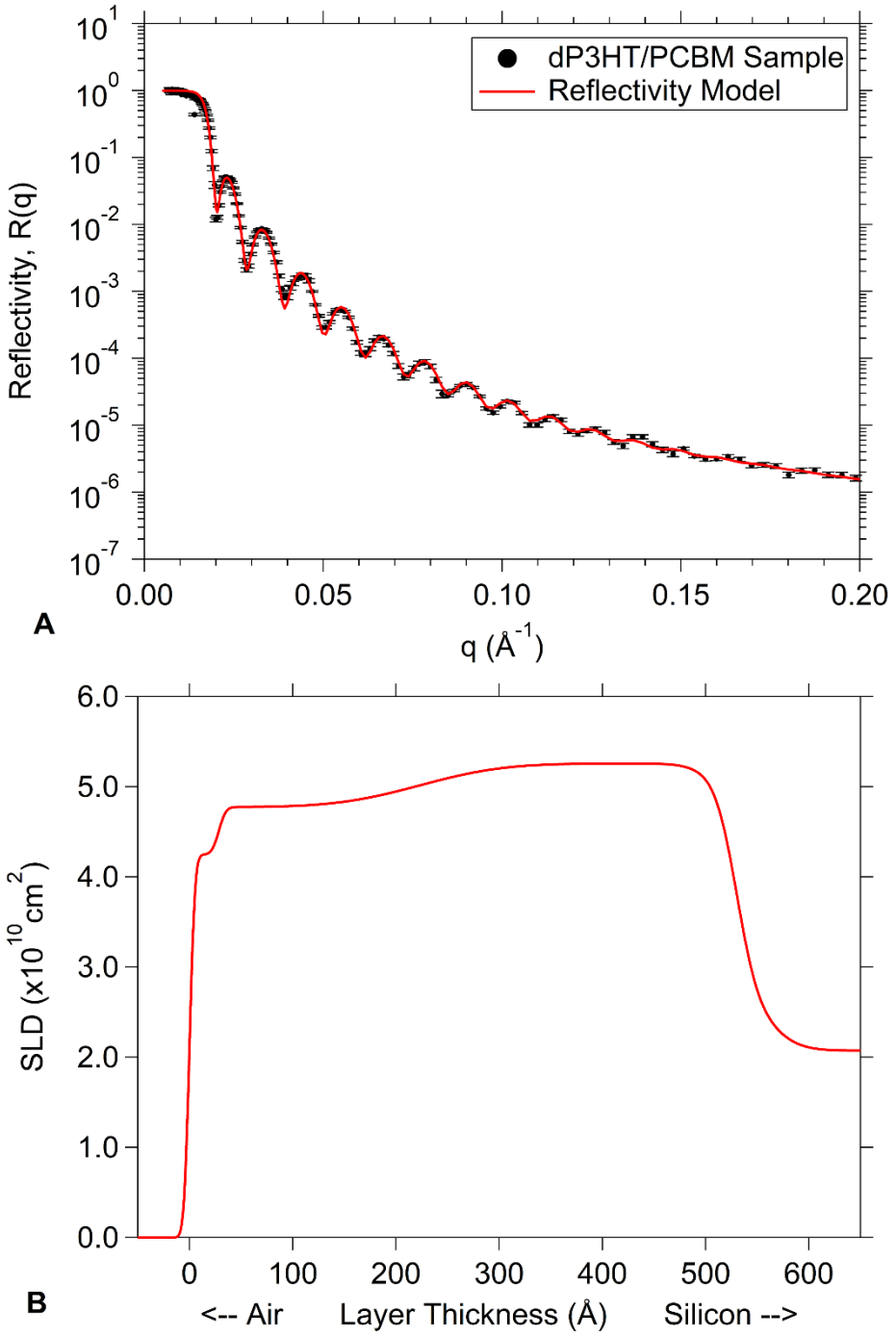

Figure S11 Neutron reflectivity data obtained from BL-4B Liquids Reflectometer at Oak Ridge National Laboratory provided by J. Keum. A blend of side-chain deuterated P3HT ($C_{10}HD_{13}S$) and PCBM was prepared using the procedure described in Shao *et al.*, 2014 and spin-coated onto a 5 mm thick silicon wafer. The reflectivity (A) and scattering length density profile (B) were modelled using the simple reflectivity tool in the Irena package for Igor Pro.

The dP3HT/PCBM film for the neutron reflectivity experiment was prepared using the procedure described in Shao *et. al*'s work. The reflectivity data obtained from BL-4B Liquids Reflectometer at Oak Ridge National Laboratory by J. Keum is shown in Figure S11A. The data was

fit using a model of four stacked layers. The volume fraction of PCBM in the layer closest to the substrate from Shao *et al.*'s work is $\phi_{PCBM} = 0.23$. The density of dP3HT is calculated to be 1.2 g/cm^3 by multiplying the density of P3HT from the literature (Lee & Dadmun, 2014), 1.1 g/cm^3, by the ratio of molar mass of dP3HT to P3HT (180.4 Da / 166.3 Da). The PCBM weight fraction is calculated using the densities of PCBM (1.5 g/cm^3) and dP3HT (1.2 g/cm^3) to be 0.27 via Equation S2.

$$\phi_{w,PCBM} = \frac{\phi_{v,PCBM}\rho_{m,PCBM}}{\phi_{v,PCBM}\rho_{m,PCBM}+(1-\phi_{v,PCBM})\rho_{m,dP3HT}} \quad \text{(S2)}$$

In Equation S2 ϕ_w indicates weight fraction, ϕ_v indicated volume fraction and ρ_m indicates mass density. Using the known SLD of PCBM, 4.3 × 10^{10} cm^{-2} from the literature (Keum *et. al*, 2013a) and the SLD of the layer closest to the substrate in Figure S11B, 5.25 × 10^{10} cm^{-2}, the SLD of dP3HT is calculated by Equation S3 to be 5.6 × 10^{10} cm^{-2}.

$$\rho_{dP3HT} = \frac{\rho_{level}-\phi_{w,PCBM}\rho_{PCBM}}{1-\phi_{w,PCBM}} \quad \text{(S3)}$$

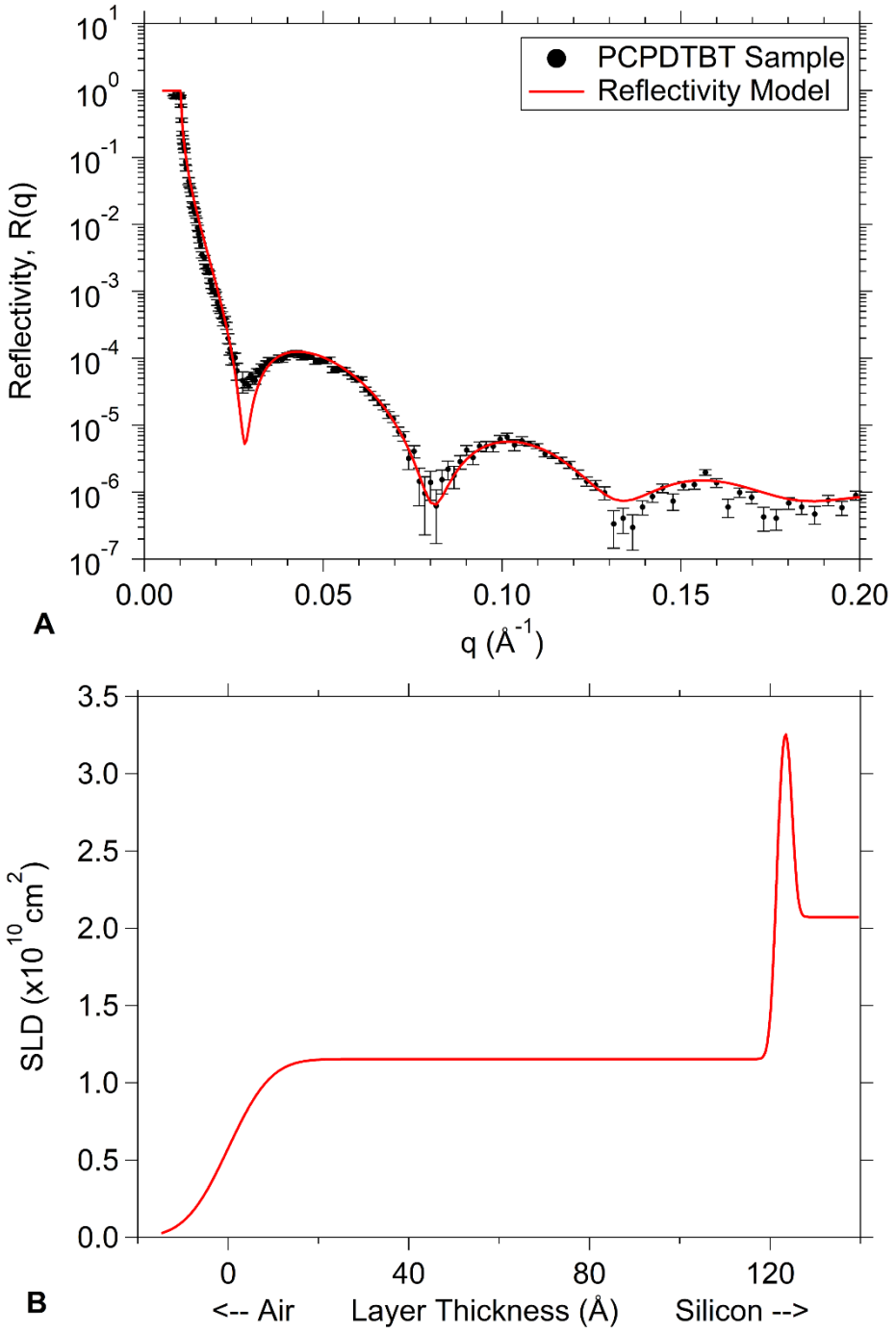

Figure S12 – Neutron reflectivity data obtained from BL-4B Liquids Reflectometer at Oak Ridge National Laboratory. A thin film of PCPDTBT was spin-coated onto a 5 mm thick silicon wafer and the reflectivity (A) and the scattering length density profile (B) were modelled using the simple reflectivity tool in the Irena package for Igor Pro.

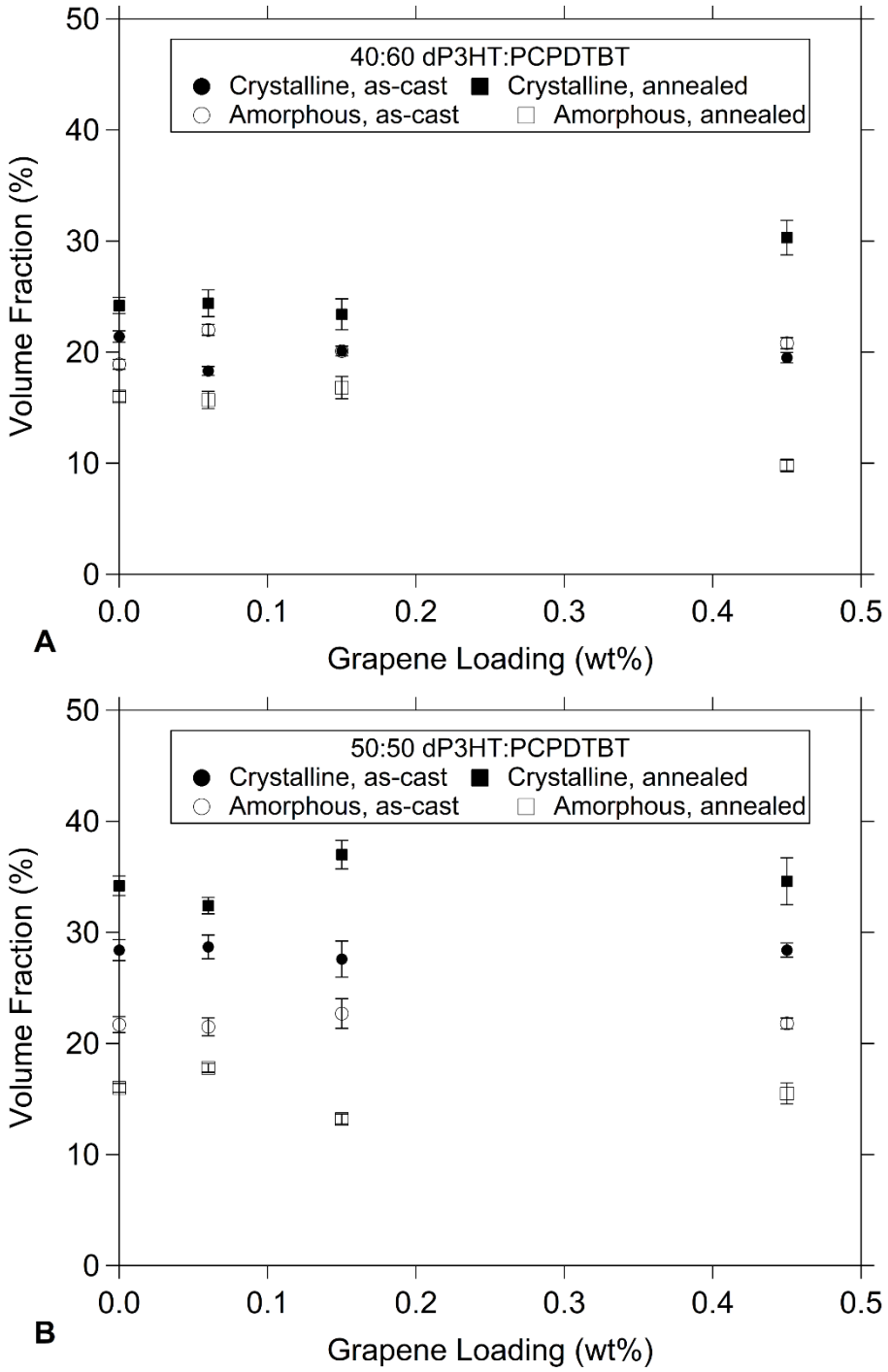

Figure S13 Crystalline (filled points) and amorphous (open points) volume fractions of dP3HT in 40:60 (A) and 50:50 (B) dP3HT/PCPDTBT films as-cast (circles) and post-anneal (squares). As expected, annealing results in increased crystalline dP3HT volume fraction. However, a significant fraction of amorphous dP3HT is present in all samples.